

Two-parameter bifurcation study of the regularized long-wave equation

O. Podvigina¹, V. Zheligovsky¹, E.L. Rempel^{2,3}, A.C.-L. Chian^{2,3,4}, R. Chertovskih²,
P.R. Muñoz^{2,5}

¹*Institute of Earthquake Prediction Theory and Mathematical Geophysics,
Russian Academy of Sciences,
84/32 Profsoyuznaya St., 117997 Moscow, Russian Federation*

²*Institute of Aeronautical Technology (IEFM/ITA),
São José dos Campos, São Paulo 12228-900, Brazil*

³*National Institute for Space Research (INPE)
and World Institute for Space Environment Research (WISER),
P.O. Box 515, São José dos Campos, São Paulo 12227-010, Brazil,*

⁴*School of Mathematical Sciences, University of Adelaide, Adelaide, SA 5005,
Australia*

⁵*Departamento de Física y Astronomía, Universidad de La Serena, Av. Cister-
nas 1200, La Serena, Chile*

Abstract

We perform a two-parameter bifurcation study of the driven-damped regularized long-wave equation by varying the amplitude and phase of the driver. Increasing the amplitude of the driver brings the system to the regime of spatiotemporal chaos (STC), a chaotic state with a large number of degrees of freedom. Several global bifurcations are found, including codimension-two bifurcations and homoclinic bifurcations involving three-tori and the manifolds of steady waves, leading to the formation of chaotic saddles in the phase space. We identify four distinct routes to STC; they depend on the phase of the driver and involve boundary and interior crises, intermittency, the Ruelle–Takens scenario, the Feigenbaum cascade, an embedded saddle-node, homoclinic and other bifurcations. This study elucidates some of the recently reported dynamical phenomena.

1 Introduction

Spatiotemporal chaos (STC) is a state of a dynamical system, characterized by the lack of order both in time and space. STC typically arises in systems strongly driven out of equilibrium, such as high Reynolds number fluid flow, or in spatially extended systems, such as large-aspect-ratio Bénard convection. STC can be defined differently as a state with a large number of degrees of freedom; their presence distinguishes STC from temporal chaos (TC), characteristic for low-dimensional attractors. Here, by degrees of freedom we understand the active spatial Fourier modes, i.e., the modes with a considerable amount of energy. An increase in the number of excited Fourier modes through nonlinear interactions implies that the spatial complexity is augmented. While the extensive study of TC has led to a substantial progress in the theory of dynamical systems (the concepts of global bifurcations, attractors and fractals have emerged in the TC theory), much less has been achieved so far in exploration of STC. This paper is devoted to the identification of the route (in other terms, of a sequence of bifurcations) leading to STC. The importance of this problem can be illustrated by the fact that transition to turbulence, a subject of interest in fluid mechanics in the last hundred years since the work of Reynolds, is an instance of transition to STC (see [10]).

Investigation of bifurcations in nonlinear partial differential equations has often been regarded as a way to understand the onset of STC (e.g., see Bohr et al. [2], who consider the onset of weak turbulence in fluids and plasmas). The usual approach consists of varying one control parameter while fixing all other system parameters. However, some bifurcations can only be observed when two parameters are varied (the so-called codimension-two bifurcations [25]). Given that much more information on codimension-one global bifurcations is available than on those of higher codimensionality, considering global bifurcations in two-parameter systems has the potential of yielding important results. Another interesting question is how the route to STC is modified when we slightly change the values of the parameters that were fixed in the one-parameter study, i.e., what are the stability properties of the route to STC under a small variation of parameters. A related question is whether a “typical” route to STC exists (at least, in a particular system under consideration), i.e. whether the route is (in some sense) unique.

In this paper, we perform a two-parameter bifurcation study of solutions

to the regularized long-wave equation (RLWE) in the presence of an external driver and linear damping, with the emphasis on how the transition to STC, on increasing the amplitude of the external driver, depends on the phase of the driver. The RLWE, also known as the Benjamin-Bona-Mahony equation, models the propagation of one-dimensional, unidirectional small-amplitude long waves in nonlinear dispersive media. It was first derived by Peregrine [31], then by Benjamin et al. [1], as an alternative to the Korteweg-de Vries equation [6]. The RLWE was employed to study the propagation of long waves in shallow waters [6], tsunami waves [38] and drift waves in a controlled nuclear fusion plasma [24]. Our approach to investigation of transition to STC is purely numerical. For an example of analytical study of Hopf and steady state bifurcations in a system of nonlinear elliptic PDEs describing a reaction-diffusion predator-prey model, see e.g. [39], where spatially nonhomogeneous periodic orbits bifurcating from the curve of the constant coexistence steady states were investigated.

The RLWE was also used as a canonical model for transition to STC and wave turbulence. He [17] explored a crisis transition from a temporally chaotic and spatially coherent state to an STC state occurring in the driven-damped RLWE on increasing the driver amplitude. This transition was subsequently investigated in [18, 19, 20, 22, 23]. More recently, Rempel and Chian [34] and Rempel et al. [35] studied the transient and intermittent dynamics in this transition to STC, showing that immediately upon the transition the system displays intermittent switching between TC and STC states (chaotic saddles). Chian et al. [4] described this intermittency in terms of amplitude and phase synchronization among spatial scales in each chaotic saddle. Galuzio et al. [11, 12] suggest that the intermittency is related to an unstable dimension variability, with unstable periodic orbits embedded in the chaotic sets losing transversal stability time and again. Finally, Chian et al. [5] claimed that the chaotic saddle responsible for the STC regime is born at the boundary between two basins of attraction due to a smooth-fractal metamorphosis. In the present paper, we identify the birth of chaotic saddles due to homoclinic bifurcations where both leading eigenvalues are complex, implying the existence of an infinite number of saddle periodic orbits. Apparently, the chaotic saddles are comprised of such unstable orbits.

In all the papers mentioned above, bifurcations of the driven-damped RLWE were studied with a single parameter, ϵ (the amplitude of the driving force), typically varied. The transition from TC to STC was investigated for only one value

of the driver phase, $\Omega = 0.65$, for which the transition takes place via an interior crisis leading to intermittency. Here, we consider the phases in the interval $0.56 \leq \Omega \leq 0.65$ and identify, on increasing ϵ , a series of codimension-one and codimension-two global bifurcations of space-periodic solutions to the RLWE. These bifurcations are responsible for dynamic transitions involving equilibrium points, periodic, quasiperiodic and chaotic orbits. The transitions found numerically include interior and boundary crises, homoclinic bifurcations, embedded saddle-node bifurcations and the Feigenbaum and Ruelle–Takens routes to chaos. We show that the transition to STC can also happen:

- via a homoclinic bifurcation;
- via a boundary crisis bifurcation, resulting in the STC attractor emerging “out of the blue”;
- an embedded saddle-node bifurcation, where the STC attractor emerges “out of the blue” as well.

Hence, we find that there is no universality in the transition to STC – in the particular system under consideration, variation of the two parameters instead of just the amplitude reveals that there exist at least four distinct routes to STC!

Our goal to construct a *two*-parameter bifurcation diagram distinguishes our work from the majority of studies aimed at exploring bifurcations in dynamical systems. While a very detailed study of bifurcations in a one-parameter family is feasible, a thorough investigation of bifurcations in a two-parameter family is difficult and very resource consuming, especially in a large-dimensional system. Moreover, it is important not to get swamped by examination of various fine details in order not to miss the global picture. For instance, the sequence of bifurcations leading to STC in RLWE for $\Omega = 0.65$ was studied in several dozens of papers (see the papers cited above and references therein), where much attention was paid to the boundary crises and intermittency — but in the present paper we show that these phenomena are not really essential. Since we are interested in the global picture, we cannot allow ourselves and do not intend to go into minute details, leaving this for future studies.

The paper comprises four sections. In Section 2, the driven-damped RLWE is presented. Section 3 reviews the definitions of the relevant global bifurcations. The bifurcations occurring in the dynamical system are discussed in section 4. The final remarks are given in section 5.

2 Equations and numerical methods

We solve the regularized long-wave equation with forcing and damping,

$$\frac{\partial \psi}{\partial t} + a \frac{\partial^3 \psi}{\partial t \partial x^2} + c \frac{\partial \psi}{\partial x} + f \psi \frac{\partial \psi}{\partial x} = -\nu \psi - \epsilon \sin(x - \Omega t), \quad (1)$$

under the periodicity condition

$$\psi(x, t) = \psi(x + 2\pi, t).$$

The equation involves six parameters, a , c , f , ν , Ω and ϵ , but only four of them are independent, because the transformations

$$t \rightarrow at, \quad c \rightarrow \alpha c, \quad f \rightarrow \alpha f, \quad \nu \rightarrow \alpha \nu, \quad \epsilon \rightarrow \alpha \epsilon, \quad \Omega \rightarrow \Omega/\alpha$$

and

$$f \rightarrow \beta f, \quad \psi \rightarrow \psi/\beta$$

do not modify the equation.

Upon changing the spatial variable to $\xi = x - \Omega t$ (i.e., in the reference frame co-moving with the external driver) equation (1) takes the form

$$\frac{\partial}{\partial t} \left[\psi + a \frac{\partial^2 \psi}{\partial \xi^2} \right] - \Omega \frac{\partial}{\partial \xi} \left[\psi + a \frac{\partial^2 \psi}{\partial \xi^2} \right] + c \frac{\partial \psi}{\partial \xi} + f \psi \frac{\partial \psi}{\partial \xi} + \nu \psi + \epsilon \sin \xi = 0. \quad (2)$$

A solution to (2) can be expanded in Fourier series,

$$\psi(\xi, t) = \sum_{k=-\infty}^{\infty} u_k(t) e^{ik\xi}. \quad (3)$$

Substitution of (3) into (2) yields a system of ordinary differential equations for the complex coefficients $u_k(t)$.

Similarly, a solution to (1) can be expanded in Fourier series

$$\psi(x, t) = \sum_{k=-\infty}^{\infty} v_k(t) e^{ikx}. \quad (4)$$

Evidently, coefficients of the two series are related:

$$u_k(t) e^{ik\Omega t} = v_k(t). \quad (5)$$

The energy of a solution is

$$E = \frac{1}{4\pi} \int_0^{2\pi} \left[\psi^2(x, t) - a^2 \left(\frac{\partial \psi(x, t)}{\partial x} \right)^2 \right] dx. \quad (6)$$

For analyzing bifurcations, (2) is more convenient than (1), because in the co-moving reference frame the attractors lose a degree of complexity (e.g., a travelling wave becomes a steady state, and a torus becomes a periodic orbit). However, the equivalent (by (5)) equation (1) is more practical for computations¹.

3 Global bifurcations

Before presenting numerical results, we review the types of global codimension-one bifurcations that occur in our system. In this section we consider a dynamical system

$$\dot{x} = f(x, \alpha), \quad f : \mathbb{R}^{n+1} \rightarrow \mathbb{R}^n, \quad f \in C^k(\mathbb{R}^n), \quad \text{where } k \geq 5, \quad (7)$$

and assume that a bifurcation occurs at a critical parameter value $\alpha = \alpha_c$.

Boundary crisis. Suppose system (7) has two attractors. Often the boundary between basins of the attractors coincides with the stable manifold of an unstable invariant set; this holds true for the RLWE, the set being just an unstable steady state. Suppose that on variation of the parameter α , the minimum distance between an attractor and its basin boundary decreases, approaching zero when $\alpha \rightarrow \alpha_c$, so that for $\alpha = \alpha_c$ the attractor collides with its basin boundary. For α slightly above α_c , the attractor turns into a transient. Trajectories starting in the basin of the former attractor typically spend a considerable time near this set, now unstable, before approaching the other coexisting attractor. Hence the set is still visible in the temporal evolution of trajectories for a positive measure set of initial conditions.

Interior crisis. Suppose an attractor collides with a stable manifold of an unstable invariant set that belongs to the attractor's basin. After the bifurcation, trajectories starting near the former attractor traverse towards the

¹For $\epsilon = 0$, (1) and (2) have a steady solution $\psi = 0$, the eigenmodes of the operator of linearization about which are e^{ikx} and $e^{ik\xi}$ with the associated eigenvalues $(-\nu - ikc)/(1 - k^2a)$ and $(-\nu - ikc)/(1 - k^2a) + i\Omega k$, respectively. For large k , (2) has eigenvalues with large imaginary parts. For a sufficiently small ϵ , the large imaginary parts persist, forcing us to proceed with tiny time steps.

invariant set along its stable manifold, continue along its unstable manifold, and finally return to a neighborhood of the former attractor. The bifurcation results in a significant enlargement of the attractor, the new attractor including the former one, the unstable invariant set and their unstable manifolds. The temporal behavior of trajectories comprising the new attractor is thus more complex than that of the trajectories comprising the old one.

The two types of crises are discussed in the monograph [29]. Note that we use the word “crisis” in a broader sense than, e.g., in [15], where it is defined as “a collision between a chaotic attractor and a coexisting unstable fixed point or a periodic orbit”.

The Ruelle–Takens route of transition to chaos. A small C^2 (C^∞) perturbation of a quasiperiodic flow on the 3-torus (the m -torus, $m \geq 3$, respectively) can result in emergence of strange Axiom A attractors [37, 28]. Hence, if the system (7) possesses a quasiperiodic attractor with three incommensurate frequencies, then a small perturbation of f in (7) changes the motion from a quasiperiodic one to a chaotic one. The respective route from a stable steady regime to a chaotic attractor involves at least three Hopf bifurcations: the first one results in the emergence of a periodic orbit, the second one turns the periodic motion into a quasi-periodic one, and in the third one a quasi-periodic regime with three incommensurate frequencies sets in. The system can become chaotic bypassing the onset of the three-frequency regime.

The **Feigenbaum scenario** for the loss of stability of a simple periodic motion consists of an infinite number of period-doubling bifurcations. The distances between consequent bifurcation points, $\alpha_n - \alpha_{n-1}$, for large n are asymptotically close to a convergent geometric progression [7, 8]. For $\alpha > \alpha_\infty = \lim_{n \rightarrow \infty} \alpha_n$, none of these cycles is stable and trajectories become chaotic. On further increasing α , stable periodic motions with different periods emerge again, but they exist in small intervals of α only. Usually one can observe cycles with triple and quintuple periods.

Homoclinic bifurcation. An orbit $\psi(t)$ of a dynamical system is called homoclinic for an equilibrium point x_0 , if it approaches x_0 for both $t \rightarrow \infty$ and $t \rightarrow -\infty$. Such an orbit is structurally unstable, and therefore in a single-parameter system it exists only for an isolated parameter value. The behavior of trajectories near the homoclinic orbit depends on the so-called leading eigenvalues of the Jacobian matrix $df(x_0)$ that are the closest ones to the imaginary

axis, in particular, on whether the eigenvalues are real or complex.

We have checked numerically that both eigenvalues in the homoclinic bifurcation in the RLWE are complex. For such a bifurcation, it was proved [30, 9, 26] that there exists a neighborhood of the homoclinic cycle in which the system has an infinite number of saddle limit cycles for all α sufficiently close to α_c . To the best of our knowledge, such a bifurcation has never been observed before in a large- (or infinite-)dimensional physical system, although an example of a system in \mathbb{R}^4 undergoing this bifurcation is presented in [14].

Embedded saddle-node bifurcation, ESN. A saddle-node bifurcation results in the appearance of a pair of steady states, one of which is stable along the direction of the critical eigenvector of df and another one is unstable. Now, suppose the pair exists for $\alpha > \alpha_c$ and emerges at $\alpha = \alpha_c$ from a steady state that belongs to a chaotic attractor (or, in other terms, is embedded in the chaotic attractor). If this steady state is stable in directions transverse to the critical eigenvector, then for $\alpha > \alpha_c$ the attractor becomes a transient and trajectories starting in the basin of the former attractor, after wandering around this now unstable set, are finally attracted by the stable steady state. In [36] the ESN bifurcation of an $\mathbf{R}^2 \rightarrow \mathbf{R}^2$ map was discussed, the arguments *ibid.* can be easily generalized for the system (7).

4 Numerical results

We have studied numerically bifurcations for $0.56 \leq \Omega \leq 0.65$, step 0.01, for ϵ increasing from 0 to 0.25, the remaining RLWE (1) parameters set to the values

$$a = -0.287, \quad c = 1, \quad f = -6 \quad \text{and} \quad \nu = 0.1. \quad (8)$$

The studies [4, 5, 12, 34, 35] focused on the value $\Omega = 0.65$, other parameters also being confined to (8) and $0 < \epsilon \leq 0.25$. We have chosen a sufficiently distant lower value $\Omega = 0.56$ so that by varying Ω we could identify several routes to STC, that are different from those found for $\Omega = 0.65$. Computations were performed with the resolution of 1024 Fourier harmonics. The results are summarized in bifurcation diagrams (figs. 1 and 10) and in tables 3 and 4. We first describe transitions occurring in the system, considering individually bifurcations that occur on varying ϵ for certain fixed Ω 's. The global picture is discussed at the end of the paper. We use small letters to label codimension-one bifurcations. They are shown by solid dots in one-parameter diagrams in fig. 1

and by lines in two-parameter diagrams in fig. 10. Codimension-two points are labelled by capital letters.

4.1 Notation

In this subsection we define the notation that is used to label attractors and invariant sets of the equation in the co-moving reference frame (2) (note that a steady state of (2) is a travelling wave of (1)). As previously shown numerically [18, 19, 23] and analytically [3], equation (2) possesses a branch of steady states. For any Ω in the interval $0.56 \leq \Omega \leq 0.65$, on increasing ϵ the steady state undergoes two saddle-node bifurcations. As a result, there exists an interval of ϵ where three steady states coexist. We label by S_l , S_m and S_h the steady states with small, medium and high energies, respectively (see fig. 1). The steady states S_m comprising the intermediate part of the branch are unstable; nothing (but S_l and S_h at the end points of the S_m branch) bifurcates from them.

We label by \mathcal{A}_l and \mathcal{A}_h the attractors that bifurcate from S_l and S_h , respectively (including the stable S_l and S_h themselves). P_l , P_h , T_l , T_h , C_l and C_h denote periodic orbits, tori and chaotic attractors bifurcating from the respective branches. $P_l(F_1)$, $P_l(F_1/2)$, $P_l(F_1/4)$, etc., are periodic orbit with the primary, halved, quartered, etc., frequencies involved in a sequence of period-doubling bifurcations (the Feigenbaum scenario). A similar notation is used for tori. A quasiperiodic regime with three main frequencies is denoted T^3 . \tilde{T}^3 denotes the chaotic attractor bifurcating from T^3 in line with the Ruelle–Takens scenario. (Since no T^3 are structurally stable, an infinitesimal perturbation, e.g., a change in the time step, can turn T^3 into \tilde{T}^3 , and hence we cannot distinguish them.) Attractors were identified by analyzing Poincaré sections, and frequency spectra of the energy (6) and of individual Fourier harmonics.

In the earlier work on the RLWE, much attention was devoted to invariant sets called *chaotic saddles* [34]. Consider a compact invariant set of a dynamical system. If the set contains at least one chaotic trajectory, it can be called chaotic. In terms of its attractiveness, the set can be an attractor (here, we mean an asymptotically stable set), a repeller (a set that becomes an attractor upon reversing time $t \rightarrow -t$), or none of these. A chaotic saddle is a compact invariant chaotic set, which is neither an attractor, nor a repeller. Chaotic saddles are important, because often they are responsible for complex transient dynamics

before a trajectory finally converges to an attractor. A chaotic attractor can become a chaotic saddle, e.g., in a boundary crisis. In this bifurcation, changes of the chaotic attractor, regarded as a set in the phase space, can be small, if not infinitesimal; the essential change is in the attractiveness properties of the set.

4.2 Identification of attractors and bifurcations

Following, e.g., [29], we identify attractors of the following types: steady state, periodic orbit, tori (with two or more independent temporal frequencies, also referred to as quasiperiodic attractor), and chaotic attractor, which is none of above. Hence, to identify an attractor, we analyse the temporal behaviour of trajectories, in particular, by considering the frequency spectra of energy or Fourier coefficients. Examples of frequency spectra are shown in fig. 2. As an additional check, we also consider Poincaré sections, which we also use to illustrate the occurring bifurcations.

Let us point out an important question not addressed here. As mentioned above, STC is characterised by a large number of degrees of freedom, which can be estimated numerically as the dimension of attractors or the number of positive Lyapunov exponents. It is therefore of interest to determine how these quantities vary on the (Ω, ϵ) plane. However, we regard this as an independent problem. Such computations are very numerically demanding, especially given that the number of degrees of freedom is large (this also raises the issues of accuracy), as indicated by the results for $\Omega = 0.65$ [4, 5].

As we have stated in the introduction, our goal is to understand the global picture without going into fine details (despite they may be important), with the emphasis on bifurcations related to the transition to STC. In particular, we do not perform a thorough investigation of bifurcations of \mathcal{A}_l : for $\Omega \geq 0.64$ (this agrees with the findings of [5] for $\Omega = 0.65$), \mathcal{A}_l undergoes a complex sequence of bifurcations, including period-doublings, some of them comprising a Feigenbaum scenario, Hopf bifurcations and foldings of the branch of attractors resulting in several saddle-node bifurcations.

A steady state can be efficiently computed by a program that solves an equation $F(x) = 0$ (we use the code from [33] based on Broyden's method), where $F(x)$ represents the r.h.s. of (2). Bifurcations of a steady state can then be determined by computing the eigenvalues of the linearisation of $F(x)$ near

the steady state. Bifurcations of periodic orbits and tori are studied by direct numerical simulations, by considering the energy spectra of the solutions and by comparing the number and values of independent frequencies before and after a bifurcation.

As in any generic system, for a fixed Ω and only ϵ varied, codimension-one bifurcations are expected to take place. All types of such bifurcations are known, and therefore it suffices to register specific features of a bifurcation to identify it. The ones listed in section 3 were identified as follows. Before a *boundary crisis*, a system possesses two attractors, and after it one of the attractors turns into a chaotic transient. A trajectory starting near the defunct attractor stays in its vicinity for a long time (see, e.g., plots shown in fig. 7), before making its way to the other attractor. Thus, a transformation of one of the attractors, on variation of a parameter, into a chaotic transient is a signature of a boundary crisis bifurcation.

An *interior crisis* is characterised by a significant enlargement of the attractor, the former attractor becoming a part of the new one. This is detected in various temporal plots (e.g., in Fig. 9 we see time intervals when the trajectory is close to the former C_l and C_h) and in Poincaré sections. The *Ruelle-Takens* route to chaos requires existence of three temporal frequencies. On a minor variation of a parameter, a chaotic behaviour turns into a quasiperiodic one due to frequency locking. The system is highly sensitive to perturbations, including those of the numerical nature, such as changing the time step or spatial resolution. A *Feigenbaum scenario* is characterised by a sequence of accumulating period-doubling bifurcations, bringing system to a chaotic state. As usual, Poincaré sections (see, e.g., fig. 8b,c, higher- ϵ regions) illustrate well the transition.

To study bifurcations involving *homoclinic and heteroclinic trajectories*, it is useful to consider the difference $\psi(t) - S_*$ between a solution $\psi(t)$ and a steady state S_* and its energy, $E(\psi(t) - S_*)$. A structurally unstable homoclinic or heteroclinic trajectory exists for an isolated parameter value. For nearby values, trajectories closely follow stable and unstable manifolds of a steady state (as, e.g., in fig. 4b for $2500 < t < 3000$), which we use as a signature.

In the *ESN* bifurcation, the critical value ϵ_j for disappearance, on decreasing ϵ , of the chaotic attractor C_h coincides with the critical value for emergence of S_m and S_l in a saddle-node bifurcation. An alternative scenario that we also observe in computations is the disappearance of C_h in a BC bifurcation at ϵ_i ,

implying coexistence of S_l and C_h for $\epsilon_i < \epsilon < \epsilon_a$.

Except for bifurcations of steady states (and sometimes periodic orbits), where critical points can be found by computing eigenvalues, in numerical studies points of bifurcations are detected by computing intervals of existence of attractors. Intervals of existence of attractors are given in tables 3 and 4, bifurcations are listed in table 1. From these tables, one can estimate critical values of ϵ for some bifurcations: for a,j,r,s or b,h,i,o,p as endpoints of intervals of existence of \mathcal{A}_l or \mathcal{A}_h , respectively; l,n,c,d and e are located between intervals where the relevant attractors (S_l and $P_l(F_1)$, $P_l(F_1)$ and $P_l(F_1/2)$, S_h and $P_h(f_1)$, $P_h(f_1)$ and $P_h(f_1, f_2)$, $P_h(f_1, f_2)$ and $P_h(f_1, f_2/2)$, respectively) exist. For example, for $\Omega = 0.56$, tables 1 and 3 imply that the critical value of the saddle-node bifurcation for disappearance of S_l is $\epsilon_a \approx 0.103$; from tables 1 and 4, the critical value for Hopf bifurcation of S_h satisfies $0.0944 < \epsilon_c < 0.0945$.

Plots of the energy (6) (fig. 1) as a function of ϵ for six values of Ω summarise bifurcations occurring in the system and show four different routes of transition to STC. When the steady states S_m , S_l and S_h are not attracting, they are shown by dashed lines. For clarity, we present only the major bifurcations. For example, for $\Omega = 0.56$ (top left panel) we show the saddle-node bifurcations resulting in emergence of $S_{l,m,h}$, a and b; the Hopf bifurcation of S_h , c; and the homoclinic bifurcation, g.

4.3 $\Omega = 0.56$ and $\Omega = 0.57$

For $\Omega = 0.56$, the steady states S_l in the lower part of the branch are always stable till the branch turns back in the saddle-node bifurcation at $\epsilon = \epsilon_a$. (Evidently, ϵ_a depends on Ω and we should write $\epsilon_a(\Omega)$, but we abbreviate this notation for the sake of simplicity.) The steady states S_h in the upper part of the branch emerge in the saddle-node bifurcation on increasing ϵ at $\epsilon = \epsilon_b$ and become unstable in the Hopf bifurcation at $\epsilon = \epsilon_c$ with emergence of a stable periodic orbit. The orbit bifurcates into a torus in another Hopf bifurcation at $\epsilon = \epsilon_d$, followed by halving of one of the basic frequencies of the torus ($\epsilon = \epsilon_e$). The next Hopf bifurcation results in the emergence of a torus with three main frequencies. For higher ϵ , in a small interval $\epsilon_f \leq \epsilon \leq \epsilon_g$ a variety of attractors was observed in computations: chaotic attractors (existing in agreement with the Ruelle–Takens scenario), periodic orbits and tori with frequencies f_1/n_1 , f_2/n_2 and f_3/n_3 , where f_j are the three frequencies of T_h^3 and n_j are integer

(see fig. 3). We attribute the respective transitions to frequency locking and do not study them in depth.

At the interval $\epsilon_f \leq \epsilon \leq \epsilon_g$, a steady state S_h has a two-dimensional unstable manifold that is attracted by \tilde{T}_h (recall that this is a generic notation for the attractors \tilde{T}_h^3 , $T_h^3(f_1/n_1, f_2/n_2, f_3/n_3)$ or $T_h^2(f_1/n_1, f_2/n_2)$). On increasing ϵ , the distance between \tilde{T}_h and the stable manifold of S_h decreases, and finally at $\epsilon = \epsilon_g$ it vanishes. Hence, at ϵ_g the stable and unstable manifolds of S_h intersect, resulting in existence of an orbit homoclinic to S_h . This scenario can be inferred from the time series of fig. 4, where the energy of the difference between an individual trajectory ψ and the steady state S_h is plotted as a function of time. For ϵ slightly smaller than ϵ_g , the trajectory ψ is confined to the attractor T_h (fig. 4a); for ϵ slightly larger than ϵ_g , the attractor is chaotic and has already collided with the stable manifold of S_h , resulting in intermittent excursions of the trajectory ψ towards S_h , during which $E(\psi - S_h)$ becomes close to zero (fig. 4b). For larger ϵ , a similar behavior is observed, with excursions becoming increasingly frequent (fig. 4c,d). We have checked numerically that the leading eigenvalues of the linearization of (2) near S_h are complex; as follows from the theory of homoclinic bifurcations, in this case there exists an infinite number of unstable periodic orbits in a neighborhood of the homoclinic cycle for ϵ close to ϵ_g .

Computations show that for $\epsilon > \epsilon_g$ the behavior is chaotic. In time series computed for an individual trajectory, well-defined signatures of close homoclinic trajectories are observed (see fig. 4,b,c) — the time intervals, during which the trajectory approaches the steady state S_h along its stable manifold, and leaves along the unstable one. In the log-linear plot, the dependence of the energy $E(\psi(t) - S_h)$ on time during these time intervals is essentially linear.

For ϵ increasing further, the energy of flows comprising C_h increases, however there are no qualitative changes in their temporal behavior (cf. figs. 4c and d), which indicates the absence of bifurcations.

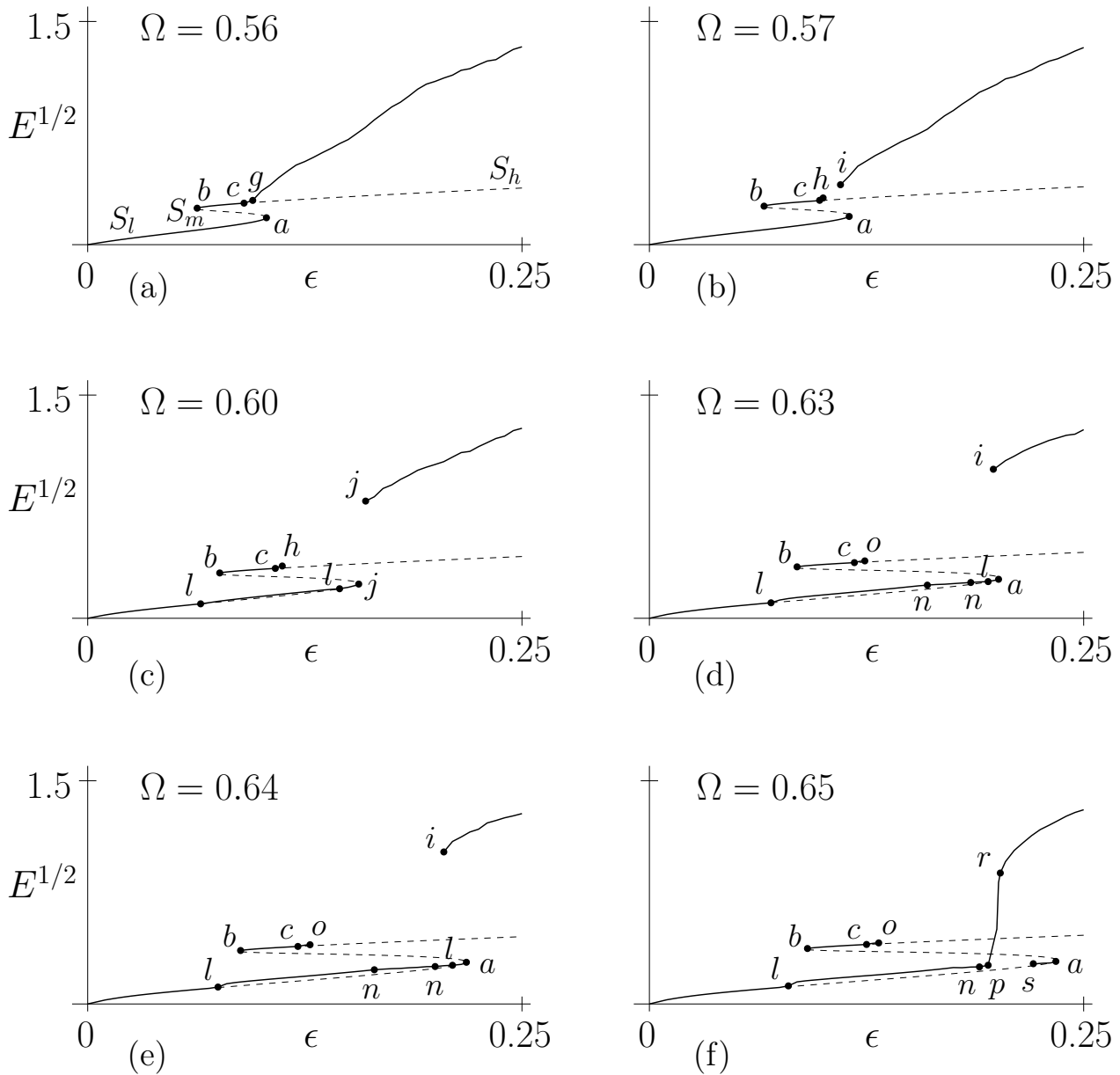


Figure 1: Bifurcation diagrams: the time-averaged square root of the energy (6) as a function of ϵ (horizontal axis) of the RLWE attractors (solid line) and unstable steady states (dashed line) for $\Omega = 0.56, 0.57, 0.60, 0.63, 0.64$ and 0.65 . Dots indicate selected bifurcation points. Labelling of the bifurcations is explained in table 2.

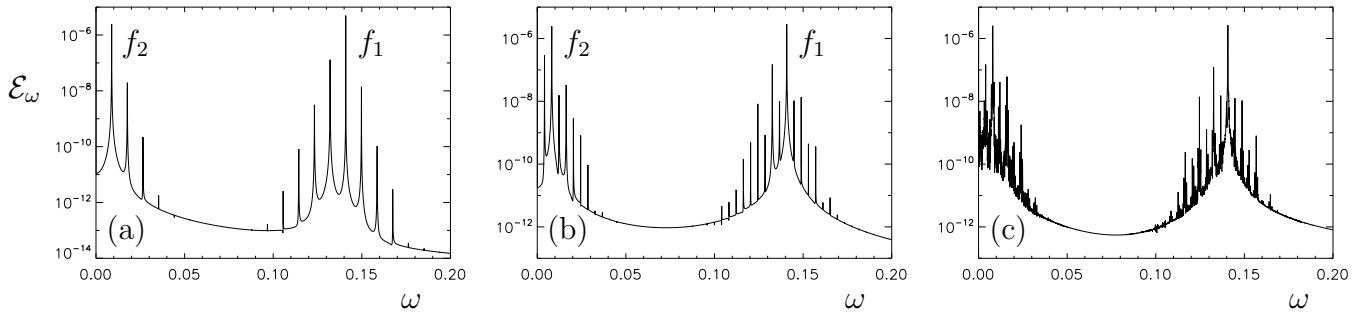


Figure 2: Frequency spectra $\mathcal{E}_\omega = |\hat{E}_\omega|^2$ of the energy $E(t) = \sum \hat{E}_\omega e^{i\omega t}$ (6) for $\Omega = 0.56$: $\epsilon = 0.0955$, attractor $T_h^2(f_1, f_2)$ (a); $\epsilon = 0.0959$, attractor $T_h^2(f_1, f_2/2)$ (b); $\epsilon = 0.096$, attractor \tilde{T}_h^3 (c). Vertical axis: \mathcal{E}_ω , horizontal axis: ω .

The route to STC for $\Omega = 0.56$ is illustrated by fig. 5, showing the evolution of the spatio-temporal structure of the attractor \mathcal{A}_h on increasing ϵ : For small ϵ , the attractor is a travelling wave, whose spatial structure is simple (fig. 5a, $\epsilon = 0.094$). When the temporal behavior becomes periodic in a Hopf bifurcation at ϵ_c , simultaneously a small-amplitude spatial oscillatory pattern emerges (fig. 5b, $\epsilon = 0.095$). (Recall, that a travelling wave solution of (1) is a steady state of (2), and when describing attractors, we assume attractors of (2).) Emergence of a second temporal frequency at ϵ_d is also accompanied by a slight enhancement of the spatial complexity of the attractor; nevertheless, for $\epsilon < \epsilon_g$ (i.e., before the homoclinic bifurcation), the spatial structure of the regime remains fairly regular. For $\epsilon > \epsilon_g$, amplitudes of spatial oscillations emerging in the Hopf bifurcations grow fast and active development of irregular spatial patterns is observed. Figs. 5c-d, $\epsilon = 0.097, 0.1$ and 0.15 , show the evolution of the chaotic attractor after the homoclinic bifurcation, as ϵ is increased. Clearly, the development of STC along this route is intimately related to the onset of temporal chaos in the solution due to its predominantly travelling-wave structure.

Spatiotemporal chaos can be characterized by a measure of the spreading of energy towards smaller scales due to nonlinear interactions, in which additional Fourier modes are excited. The spectral average has been frequently used in this context, defined as $\sqrt{N^2} = \sqrt{\sum_{k=0}^{\infty} k^2 |v_k|^2 / \sum_{k=0}^{\infty} |v_k|^2}$, where v_k denotes the k -th Fourier coefficient. In other words, the spectral average is just the enstrophy of a flow normalized by the kinetic energy, or it can be also regarded as the average Fourier mode amplitude weighted by the wave number [13, 21, 27]. Figure 6 depicts the time variation of the spectral average for the six regimes

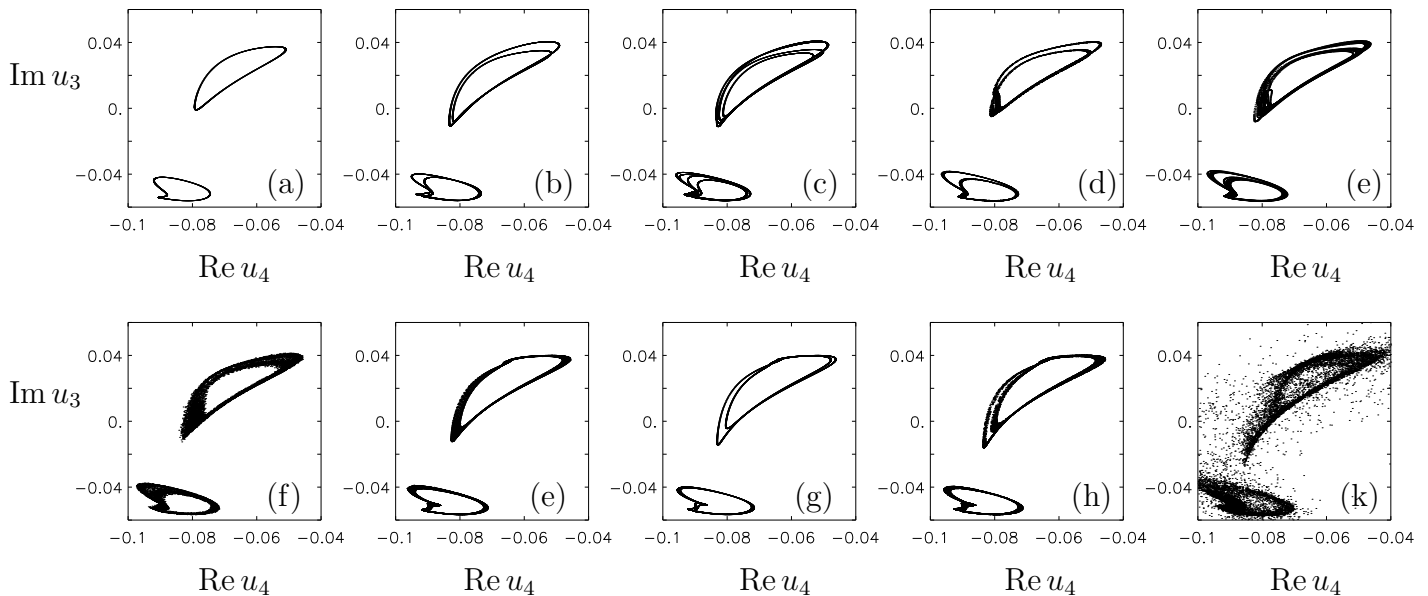


Figure 3: Poincaré sections $\text{Re } u_3 = 0.03$ for $\Omega = 0.56$, $\epsilon = 0.0955$, attractor $T_h^2(f_1, f_2)$ (a); 0.0959, $T_h^2(f_1, f_2/2)$ (b); 0.09595, $T_h^2(f_1, f_2/4)$ (c); 0.09598, $T_h^3(f_1, f_2/2, f_3)$ (d); 0.09599, $T_h^2(f_1, f_2/16)$ (e); 0.096, T_h^3 (f); 0.0963, $T_h^3(f_1, f_2, f_3)$ (g); 0.09634, $T_h^2(f_1, f_2/2)$ (h); 0.09635, $T_h^3(f_1, f_2/2, f_3)$ (j); and 0.09636, C_h (k). Vertical axis: $\text{Im } u_3$; horizontal axis: $\text{Re } u_4$.

shown in fig. 4. Note that energy is progressively spread toward higher wave numbers as ϵ is increased, with a jump of almost an order of magnitude at $\epsilon = 0.15$, where STC is strongly developed.

For $\Omega = 0.57$, similarly to $\Omega = 0.56$, the steady states S_l constituting the lower part of the branch are stable. The upper part of the branch, also as for $\Omega = 0.56$, undergoes three Hopf bifurcations interrupted by halving of one of the frequencies. As a result, a quasi-periodic regime with three main frequencies, T_h^3 , emerges.

The next bifurcation has no analogues for $\Omega = 0.56$. When T_h^3 is attracting, the system possesses two unstable steady states, S_h and S_m . The unstable manifold of S_h is attracted by T_h^3 . For $\Omega = 0.56$, the torus T_h^3 intersects with $W^s(S_h)$, giving rise to existence (just for an isolated value ϵ_g) of an orbit homoclinic to S_h . For $\Omega = 0.57$, the attractor, T_h^3 , intersects with $W^s(S_m)$, resulting in the emergence of a heteroclinic orbit from S_h to S_m , that also exists only for $\epsilon = \epsilon_h$ (a heteroclinic connection to a saddle is not structurally stable in a generic system). Existence of this heteroclinic orbit was confirmed numerically by investigating trajectories for ϵ close to ϵ_h . Trajectories on the unstable (two-dimensional) manifold of S_h were traced by computing the unstable subspace

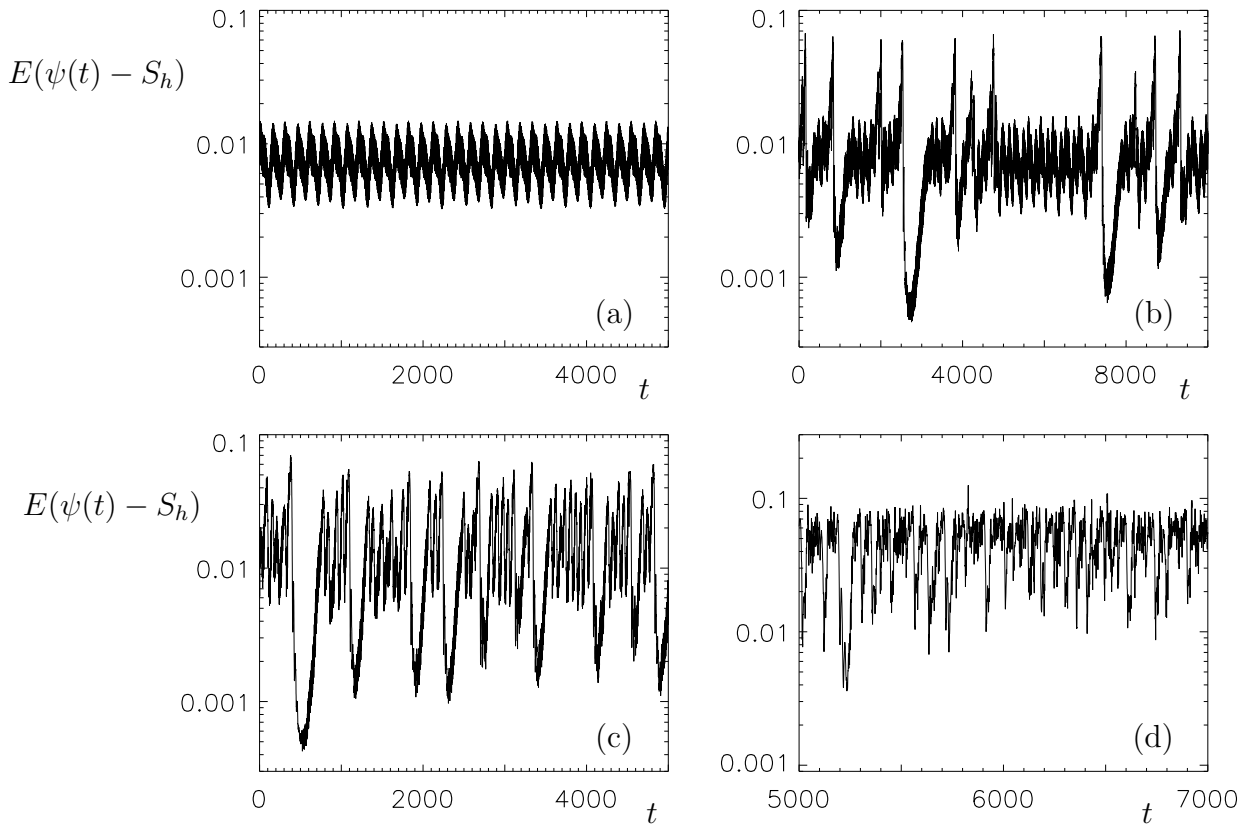


Figure 4: The discrepancy $E(\psi(t) - S_h)$ (vertical axis) for $\Omega = 0.56$, $\epsilon = 0.0963$ (a), 0.09636 (b), 0.1 (c) and 0.15 (d). Horizontal axis: time t .

of S_h and taking initial conditions in this subspace near S_h . The computations show that for $\epsilon < \epsilon_h$ these trajectories are attracted by T_h^3 , i.e., the unstable manifold of S_h is attracted by T_h^3 . Hence, the intersection of T_h^3 with $W^s(S_m)$ implies existence of a heteroclinic trajectory $S_h \rightarrow S_m$, which passes near former T_h^3 . For $\epsilon > \epsilon_h$ such trajectories go toward (unstable) S_m .

The steady state S_m has an one-dimensional unstable manifold. For ϵ slightly smaller than ϵ_h , one branch of the manifold is attracted by T_h^3 , another one by the stable S_l . For $\epsilon > \epsilon_h$, the torus T_h^3 is unstable, a trajectory starting near the torus is bound for the (unstable) S_m , and subsequently approaches S_l following the unstable manifold of S_m (see fig. 7a).

Further on, in some interval $\epsilon_h < \epsilon < \epsilon_i$ the only attractor is the stable S_l . For larger ϵ , coexistence of attractors takes place again. One of the attractors is C_h that was found for $\Omega = 0.56$. For the largest considered $\epsilon = 0.25$, C_h is an attractor for all considered Ω . On decreasing ϵ from this value, for $\Omega \geq 0.57$ it becomes unstable and turns into a chaotic saddle. For $\Omega = 0.57$, it loses

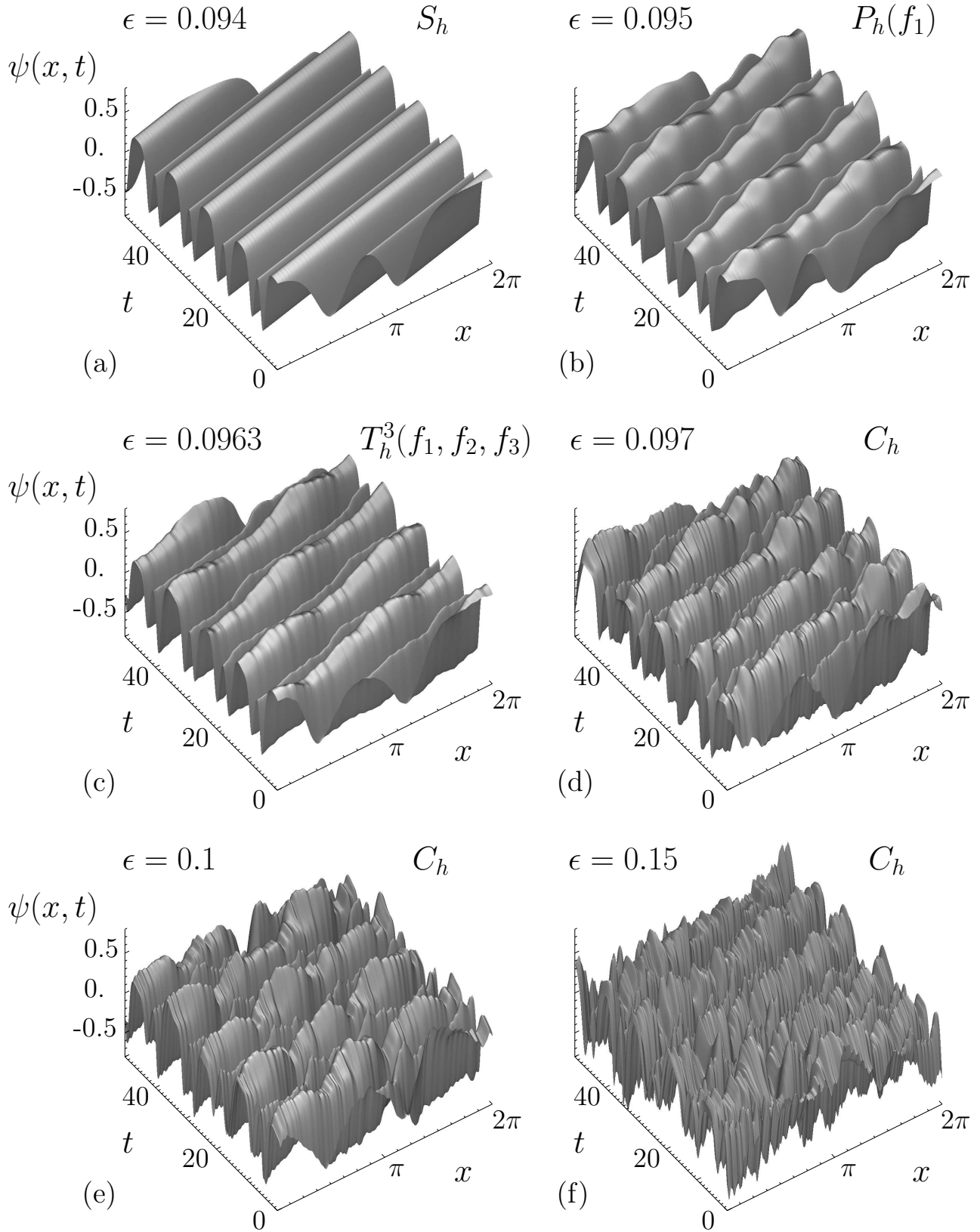


Figure 5: The route to STC for $\Omega = 0.56$: enhancement of complexity of spatio-temporal patterns in the regimes $\psi(x, t)$ on increasing ϵ . The attractors are: S_h for $\epsilon = 0.094$; $P_h(f_1)$ for $\epsilon = 0.095$; $T_h^3(f_1, f_2, f_3)$ for $\epsilon = 0.0963$; C_h for $\epsilon = 0.097, 0.1$ and 0.15 .

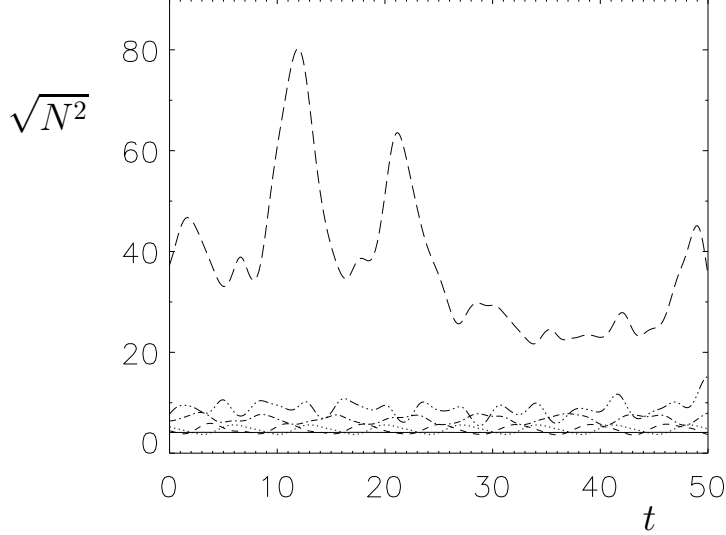


Figure 6: Time variation of the spectral average $\sqrt{N^2}$ for $\epsilon = 0.094$ (solid line), $\epsilon = 0.095$ (dotted line), $\epsilon = 0.0963$ (dashed line), $\epsilon = 0.097$ (dash-dot line), $\epsilon = 0.1$ (dash-dot-dot-dot line), and $\epsilon = 0.15$ (long dash). The attractors are: S_h for $\epsilon = 0.094$; $P_h(f_1)$ for $\epsilon = 0.095$; $T_h^3(f_1, f_2, f_3)$ for $\epsilon = 0.0963$; C_h for $\epsilon = 0.097, 0.1$ and 0.15 .

stability at $\epsilon = \epsilon_i$ via a boundary crisis. Note, that the time series of the discrepancy $E(\psi(t) - S_m)$ shown in fig. 7b does not have a minimum before the trajectory converges to S_l . This indicates that for $\epsilon = \epsilon_i$ the boundary crisis is due to the collision of the attractor with the stable manifold of S_l , in contrast with the case $\epsilon = \epsilon_h$, where it is due to the collision with the stable manifold of S_m . Similarly, for larger Ω the boundary crisis of T_h^3 is due to the collision with the stable manifold of S_m (note e.g. the minimum in fig. 7c) and the boundary crisis of C_h is due to the collision with the stable manifold of \mathcal{A}_l (chaotic attractor for $\Omega = 0.64$ shown in fig. 7d).

The proposed boundary crises scenarios are based on monitoring the time series alone. The precise characterization of crisis due to the collision of the chaotic attractor with the stable manifold of a saddle orbit is cumbersome in such a high-dimensional phase space, and we leave it for future works.

4.4 $\Omega = 0.58, 0.59, 0.60$ and 0.61

For such Ω the dependence on ϵ is similar, except for now:

- The attractors C_h and S_l do not coexist any more. This happens because on decreasing ϵ the attractor C_h became now unstable in an ESN bifurcation, and not in a boundary crisis. Occurrence of the ESN bifurcation rules out the

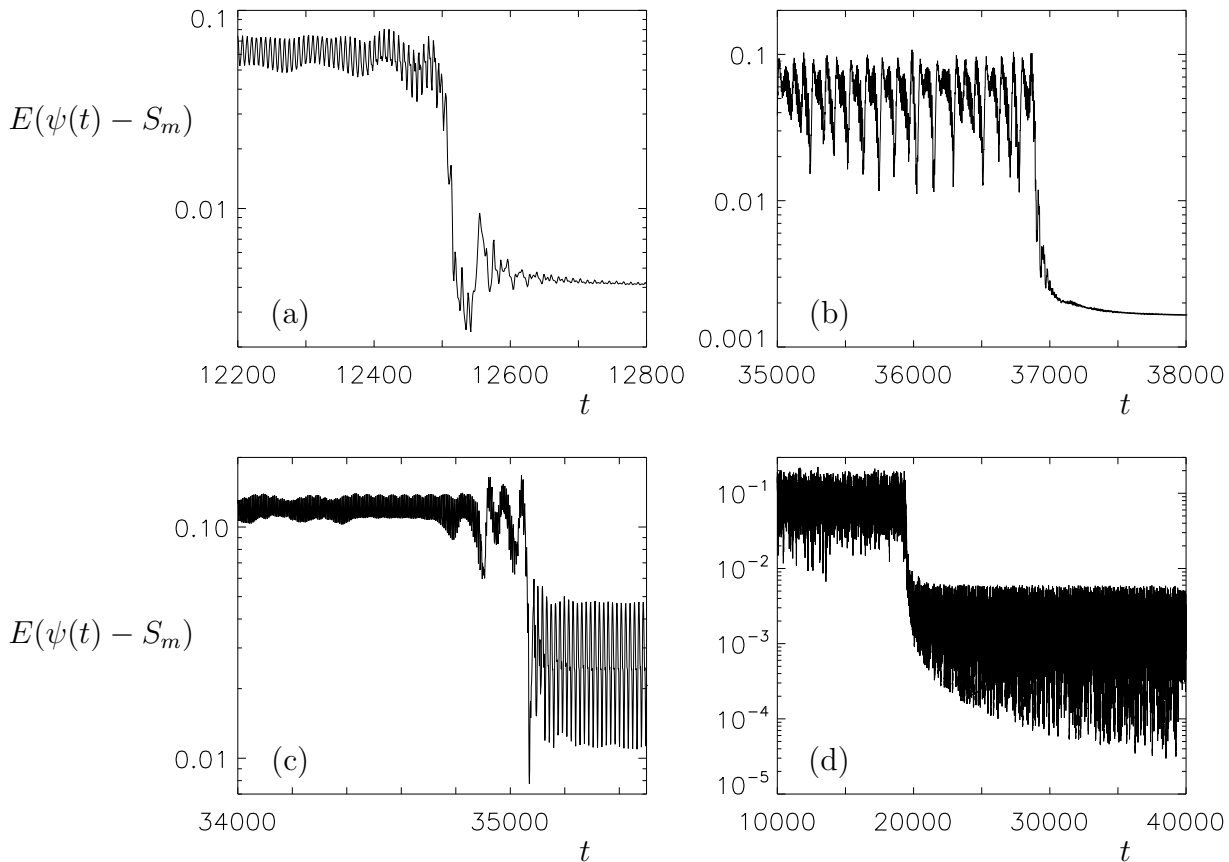


Figure 7: The discrepancy $E(\psi(t) - S_m)$ (vertical axis) for $\Omega = 0.57$, $\epsilon = 0.1001$ (a) and 0.109 (b); $\Omega = 0.64$, $\epsilon = 0.12828$ (c) and 0.2024 (d). Horizontal axis: time t .

coexistence of multiple attractors for the following reason. Consider the critical value $\epsilon_{\text{crit}}(\Omega)$ for the disappearance of S_l in the saddle-node bifurcation. When for $\epsilon = \epsilon_{\text{crit}}(\Omega)$ the distance between C_h and $S_l = S_m$ is non-zero, the bifurcation does not affect C_h , and C_h disappears at a smaller $\epsilon = \epsilon_i$ in a boundary crisis. If this distance is zero, then C_h disappears at $\epsilon = \epsilon_{\text{crit}}(\Omega) = \epsilon_j$ in the ESN bifurcation.

- The steady states S_l become unstable in a Hopf bifurcation. Two such bifurcations occur. On increasing ϵ , a periodic orbit, P_l , emerges from S_l in a forward Hopf bifurcation. On further increasing ϵ , a backward Hopf bifurcation occurs, in which P_l turns into a steady state S_l . The periodic orbit P_l is always stable.

4.5 $\Omega = 0.62$

For $\Omega = 0.62$, the bifurcations are similar to those observed for $\Omega = 0.61$, except for now:

- The attractors C_h and S_l coexist again in the interval $\epsilon_i < \epsilon < \epsilon_a$, C_h suffering a boundary crisis at $\epsilon = \epsilon_i$ as it turns into a chaotic saddle;
- The branch of the periodic orbits P_l folds. This creates two parts of the P_l branch, that consist of stable orbits, terminate in saddle-node bifurcations and coexist in the interval $\epsilon_m < \epsilon < \epsilon'_m$. For all considered $\Omega \geq 0.62$ several (two or three) branches of attractors \mathcal{A}_l coexist in certain intervals of ϵ .

4.6 $\Omega = 0.63$

The difference with the sequence of bifurcations for $\Omega = 0.62$ is in that:

- Attractors from the \mathcal{A}_h family undergo fewer bifurcations before disappearing in a boundary crisis, namely, now no tori with three main frequencies emerge and $T_h(f_1, f_2/2)$ becomes unstable due to a boundary crisis.
- The periodic orbit P_l now undergoes several forward and backward period-doubling bifurcations. The respective sequence of attractors is

$$P_l(F_1) \rightarrow P_l(F_1/2) \rightarrow P_l(F_1/4) \rightarrow P_l(F_1/2) \rightarrow P_l(F_1)$$

for one branch of \mathcal{A}_l , and $P_l(F_1) \rightarrow P_l(F_1/2)$ for another branch. For $\Omega \geq 0.63$ the bifurcations of \mathcal{A}_l are shown in the Poincaré maps (fig. 8).

4.7 $\Omega = 0.64$

Now, the behavior of attractors bifurcating from S_l is much more complex. P_l undergoes a Hopf bifurcation, forward and backward period-doubling cascades (the complete Feigenbaum scenario takes place twice, for increasing and decreasing ϵ) and saddle-node bifurcations, see fig. 8(c). Otherwise, the diagram is similar to the one for $\Omega = 0.63$.

4.8 $\Omega = 0.65$

Compared to $\Omega = 0.64$, significant changes in the sequence of bifurcations are observed (see fig. 3 in Chian et al. [5]). The attractors bifurcating from the lower branch, \mathcal{A}_l , do not exist in the whole interval of existence of S_l (see figs. 1 and 8c). On increasing ϵ , at some $\epsilon = \epsilon_p$, the chaotic attractor C_l

disappears, apparently in a collision with the stable manifold of S_m , and turns into a temporally chaotic saddle. For $\epsilon_p < \epsilon < \epsilon_r$ none of the attractors belongs to the \mathcal{A}_l or \mathcal{A}_h families. The bifurcation at $\epsilon = \epsilon_p$ is an interior crisis of \mathcal{A}_l (on increasing ϵ), the bifurcation at $\epsilon = \epsilon_r$ is an interior crisis of \mathcal{A}_h (on decreasing ϵ). As a result of the two crises, a larger attractor is formed for $\epsilon_p < \epsilon < \epsilon_r$, that involves the former \mathcal{A}_l and \mathcal{A}_h , and the intersection of their stable and unstable manifolds. A typical intermittent (see refs. [4, 34, 35]) temporal behavior of trajectories is shown in fig. 9, where for long times a trajectory stays close either to C_h (higher values of $E(\psi(t) - S_m)$), or to C_l (lower values of $E(\psi(t) - S_m)$). Note significant increase of the energy over a short interval of ϵ between two interior crisis bifurcations, the points “p” and “r” in fig. 1. The bifurcations for this control parameter were studied in detail by Chian *et al.* [5], where the intermittency shown in fig. 9 was explained in terms of regime switching between a temporally chaotic saddle and a spatiotemporally chaotic saddle. At $\epsilon = \epsilon_s$ the attractor C_l emerges “out of the blue” (a boundary crisis of C_l occurs on decreasing ϵ).

4.9 Two-parameter bifurcation diagram

The results are summarized in the bifurcation diagram (fig. 10), compiled from the numerical results presented in the previous section. The notation for bifurcations is explained in tables 1 and 2. In the area bounded by the lines “p” and “r” there are no attractors from the families \mathcal{A}_l and \mathcal{A}_h . This area represents the intermittency regime illustrated in fig. 9. Note also a codimension-two bifurcation point (labeled A) in which a homoclinic bifurcation and two boundary crisis bifurcations (of T_h and C_h) occur simultaneously. This point can be regarded as an organizing center for the nearby dynamics; future studies of this codimension-two bifurcation will clarify the transitions occurring in the dynamical system governed by the RLWE.

5 Conclusion

Many bifurcation studies employing the RLWE were conducted in the past two decades, aimed at investigating the transition to wave turbulence (see the references cited in the Introduction). In all these studies of transition to STC in the RLWE, only the amplitude of the driver, ϵ , was varied, with other param-

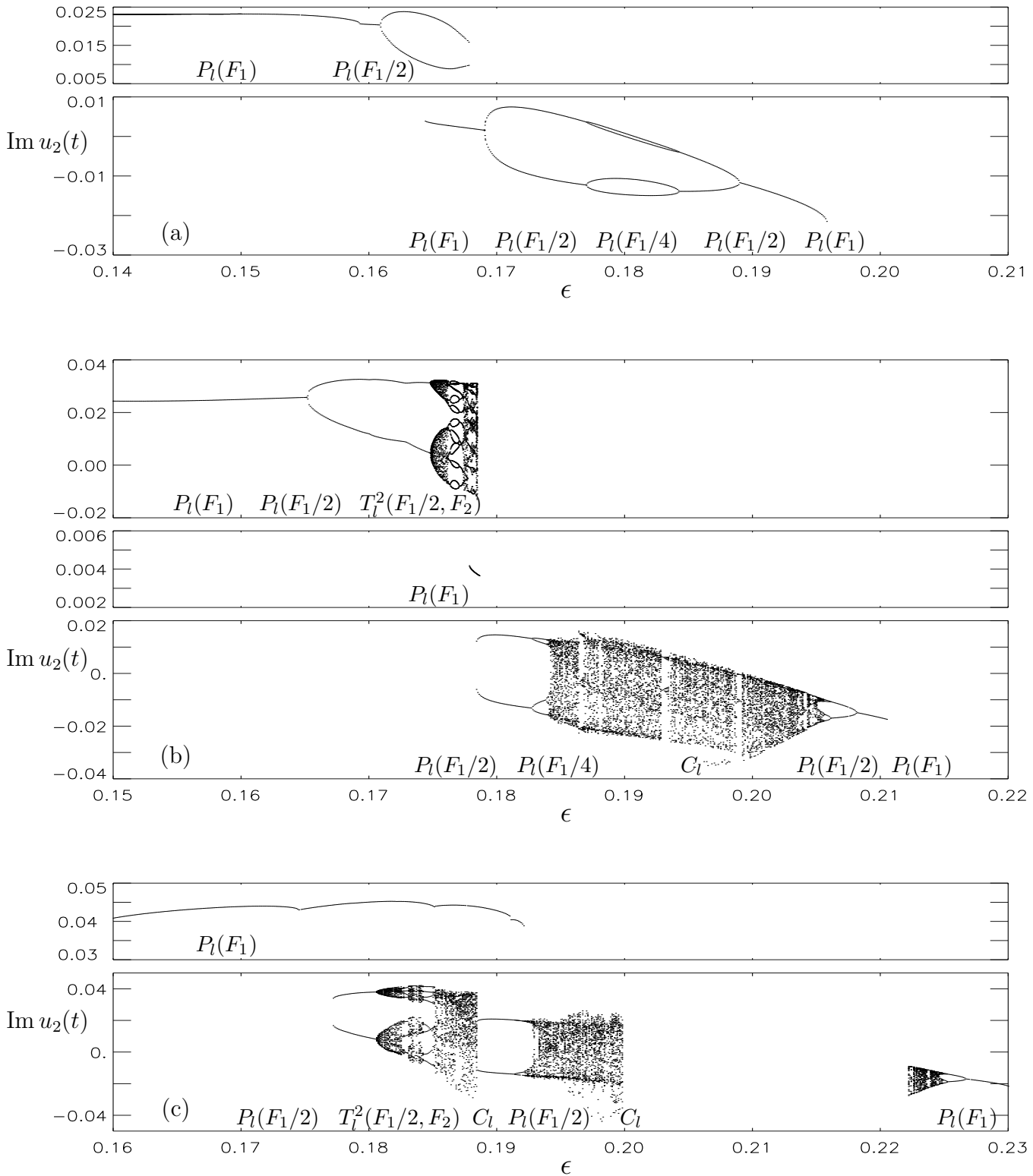


Figure 8: Poincaré sections $\text{Im } u_1(t) = 0.02$ of the attractors from the family \mathcal{A}_l , $d \text{Im } u_1(t)/dt > 0$, for $\Omega = 0.63$ (a), 0.64 (b) and 0.65 (c). Vertical axis: $\text{Im } u_2(t)$; horizontal axis: ϵ . When attractors coexist, they are shown in different plates.

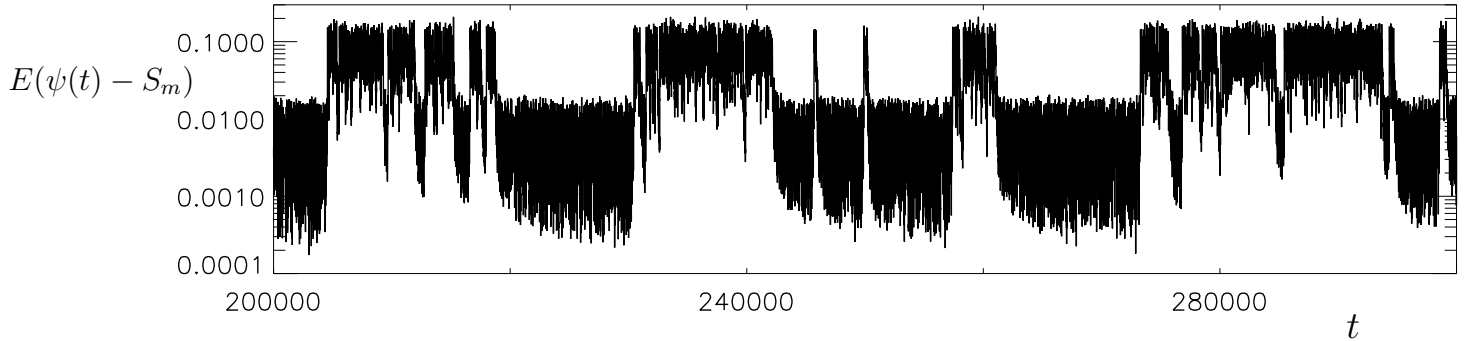


Figure 9: Intermittent temporal behavior of $E(\psi(t) - S_m)$ (vertical axis) for $\Omega = 0.65$ and $\epsilon = 0.2001$. Horizontal axis: time t .

eters set to the values (8) and $\Omega = 0.65$. The transition, via an interior crisis and intermittency, was examined in detail (see [5] and references therein). We considered the behavior of the dynamical system for the amplitude and phase of the driver in the intervals $0 < \epsilon \leq 0.25$ and $0.56 \leq \Omega \leq 0.65$, respectively.

For small ϵ , the attractor is a travelling wave, while for sufficiently large ϵ (in particular, this is always the case for $\epsilon = 0.25$), the attractor is chaotic both in time and space. For different values of Ω , routes to this regime, i.e. the sequences of bifurcations, are distinct. We have found four types of the transition. One is the route via intermittency, thoroughly investigated in the previous studies. Another route is via a homoclinic bifurcation, in which the chaotic attractor emerges in the vicinity of a structurally unstable homoclinic orbit (a codimension-one bifurcation). In the third and fourth routes to STC, the chaotic attractor emerges “out of the blue” as the amplitude of the driver is increased. Alternatively, these bifurcations can be regarded as a boundary crisis or an ESN bifurcation of the chaotic attractor on decreasing the driver amplitude.

In the bifurcation diagram, we see a codimension-two junction point, in which three lines, that indicate the homoclinic bifurcation and two boundary crisis bifurcations, are meeting (the point is marked as A in fig. 10).

Since all the three bifurcations play important roles in transition to STC, a low-dimensional dynamical system constructed by the center manifold reduction at this codimension-two point is likely to be useful for understanding the nature of the codimension-two bifurcation: the reduced system is likely to exhibit a behavior that is qualitatively similar to the one of the original system even far away (in the space of parameters) from the bifurcation point, provided advanced reduction techniques are employed (such as [32]). A possible continuation of

the present study is therefore construction of a low-dimensional reduction and investigation of bifurcations in this dynamical system.

We also note that we did not analyze the details of transition to STC for the three new routes as thoroughly as it was done for the transition via intermittency; this line of investigation is also left for future studies. A yet another open question is what kind of transitions to STC we will see for Ω outside the considered interval, or on varying the remaining parameters, a , c , f and/or ν , that have been fixed in the present study. We believe our two-parameter study of the RLWE can be used as a roadmap for further in-depth investigations of the different routes to temporal chaos and spatiotemporal chaos — the ones briefly discussed here, as well as the new ones to be identified in the future work.

Acknowledgements

OP, VZ, ELR, RC and PRM acknowledge financial support from FAPESP (grants 2012/22285-4, 2012/22243-0, 2013/22314-7, 2013/01242-8 and 2011/10466-1, respectively). ELR and ACLC acknowledge financial support from CAPES and CNPq (Brazil).

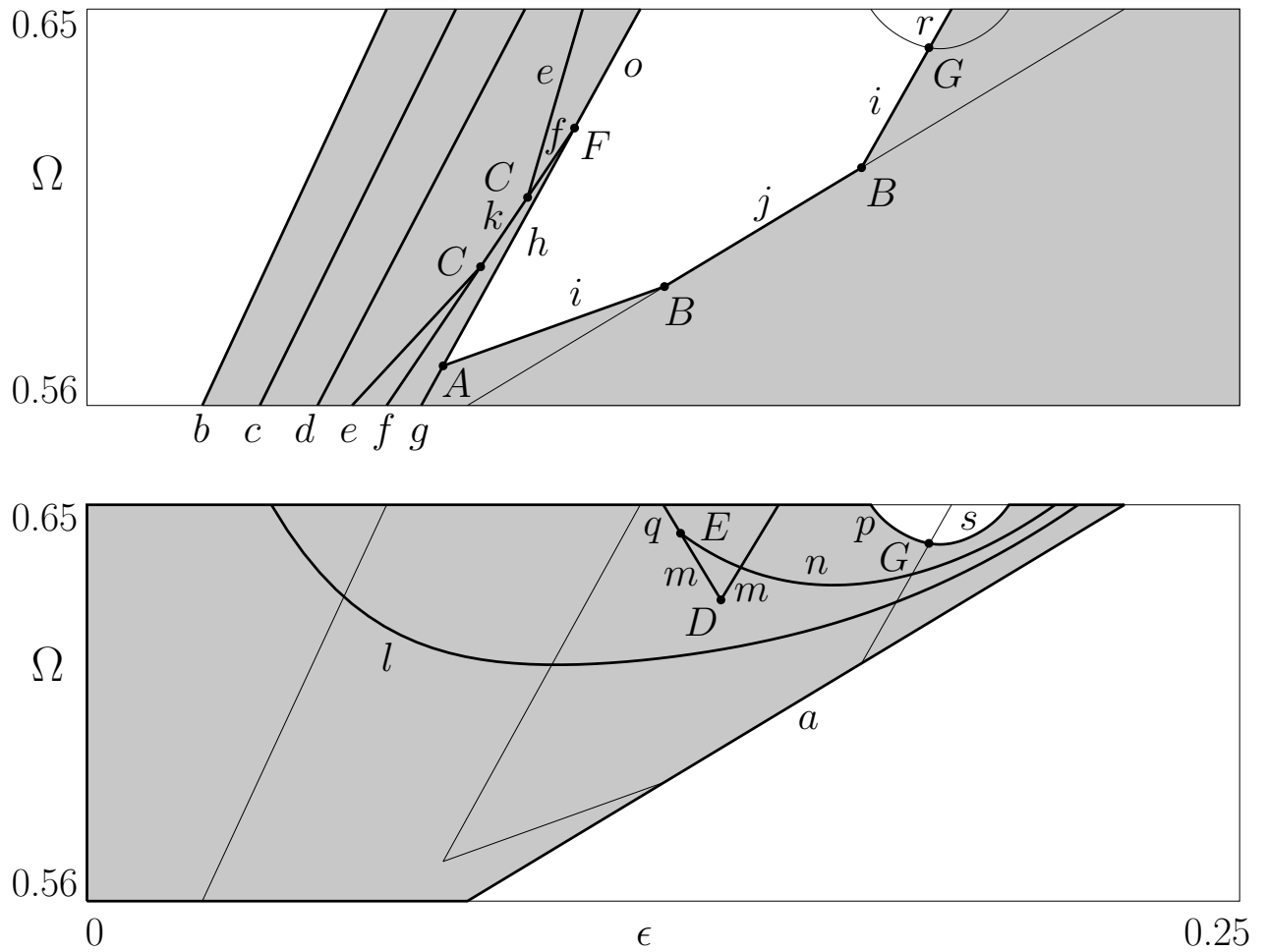


Figure 10: The global bifurcation diagram showing attractors of the families \mathcal{A}_l (lower plate) and \mathcal{A}_h (upper plate). Horizontal axis: ϵ ; vertical axis Ω . The diagram is not in scale in any direction and only the major bifurcations are shown. Bold lines denote codimension-one bifurcations and dots codimension-two bifurcations. The areas of existence of the attractors are shaded. Thin lines indicate the areas of existence of attractors from the opposing family.

Table 1. Codimension-one bifurcations shown in fig. 10.

Label	Bifurcation
<i>a</i>	saddle-node, birth of S_l and S_m (on decreasing ϵ)
<i>b</i>	saddle-node, birth of S_h and S_m (on increasing ϵ)
<i>c</i>	Hopf, $S_h \rightarrow P_h(f_1)$ (on increasing ϵ)
<i>d</i>	Hopf, $P_h(f_1) \rightarrow T_h(f_1, f_2)$ (on increasing ϵ)
<i>e</i>	period-doubling, $T_h(f_1, f_2) \rightarrow T_h(f_1, f_2/2)$ (on increasing ϵ)
<i>f</i>	Hopf, $T_h(f_1, f_2/2) \rightarrow T_h^3(f_1, f_2/2, f_3)$ (on increasing ϵ)
<i>g</i>	homoclinic, $T_h^3 \rightarrow C_h$ (on increasing ϵ)
<i>h</i>	boundary crisis of \tilde{T}_h^3 (on increasing ϵ)
<i>i</i>	boundary crisis of C_h (on decreasing ϵ)
<i>j</i>	ESN, instability of C_h due to birth of S_l (on decreasing ϵ)
<i>k</i>	Hopf, $T_h(f_1, f_2) \rightarrow T_h^3(f_1, f_2, f_3)$ (on increasing ϵ)
<i>l</i>	Hopf, $S_l \rightarrow P_l(F_1)$
<i>m</i>	saddle-node, birth of $P_l(F_1)$ and its unstable counterpart
<i>n</i>	period-doubling, $P_l(F_1) \rightarrow P_l(F_1/2)$
<i>o</i>	boundary crisis of $\tilde{T}_h(f_1, f_2/2)$ (on increasing ϵ)
<i>p</i>	interior crisis of C_l (on increasing ϵ)
<i>q</i>	saddle-node, birth of $P_l(F_1/2)$ and its unstable counterpart
<i>r</i>	interior crisis of C_h (on decreasing ϵ)
<i>s</i>	boundary crisis of C_l (on decreasing ϵ)

Table 2. Codimension-two bifurcations shown in fig. 10.

Label	Bifurcations
<i>A</i>	homoclinic and boundary crisis bifurcations of $T_h^3(f_1, f_2/2, f_3)$
<i>B</i>	boundary crisis of C_h and saddle-node of S_l imbedded in C_h
<i>C</i>	frequency-halving, $T_h(f_1, f_2) \rightarrow T_h(f_1, f_2/2)$ and Hopf, $T_h(f_1, f_2/2) \rightarrow T_h^3(f_1, f_2/2, f_3)$
<i>D</i>	two saddle-node bifurcations of $P_l(F_1)$
<i>E</i>	saddle-node and frequency-halving of $P_l(F_1)$
<i>F</i>	Hopf and boundary crisis of $T_h(f_1, f_2/2)$
<i>G</i>	boundary crises of C_l and C_h

References

- [1] Benjamin T.B., Bona J.L., Mahony J.J. Model equations for long waves in nonlinear dispersive systems. *Phil. Trans. R. Soc. London, Ser. A*, **272**, 1972, 47-78.
- [2] Bohr T., Jensen M.H., Paladin G., Vulpiani A. *Dynamical systems approach to turbulence*. Cambridge Univ. Press, 1998.
- [3] Chertovskih R., Chian A.C.-L., Podvigina O., Rempel E.L., Zheligovsky V. Existence, uniqueness and analyticity of space-periodic solutions to the regularised long-wave equation. *Advances in differential equations*, **19**, 2014, 725-754 [<http://arxiv.org/abs/1305.1813>].
- [4] Chian A.C.-L., Miranda R.A., Rempel E.L., Saiki Y., Yamada M. Amplitude-phase synchronization at the onset of permanent spatiotemporal chaos. *Phys. Rev. Lett.*, **104**, 2010, 254102.
- [5] Chian A.C.-L., Muñoz P.R., Rempel E.L. Edge of chaos and genesis of turbulence, *Phys. Rev. E*, **88**, 2013, 052910.
- [6] Dodd R.K., Eilbeck J.C., Gobbon J.D., Morris H.C. *Solitons and nonlinear wave equations*. Academic, London, 1982.
- [7] Feigenbaum M.J. Quantitative universality for a class of non-linear transformations. *J. Stat. Phys.*, **19**, 1978, 25-52.
- [8] Feigenbaum M.J. The universal metric properties of nonlinear transformations. *J. Stat. Phys.*, **21**, 1979, 669-706.
- [9] Fowler A.C., Sparrow C.T. Bifocal homoclinic orbits in four dimensions. *Nonlinearity*, **4**, 1991, 1159-1182.
- [10] Frisch U. *Turbulence, the legacy of A.N. Kolmogorov*. Cambridge Univ. Press, 1995.
- [11] Galuzio P.P., Lopes S.R., Viana R.L. Two-state on-off intermittency and the onset of turbulence in a spatiotemporally chaotic system. *Phys. Rev. Lett.*, **105**, 2010, 055001.

- [12] Galuzio P.R., Lopes S.R., Viana R.L. Two-state on-off intermittency caused by unstable dimension variability in periodically forced drift waves. *Phys. Rev. E*, **84**, 2011, 056211.
- [13] Galuzio P.P., Viana R.L., Lopes S.R. Control of extreme events in the bubbling onset of wave turbulence, *Phys. Rev. E*, **89**, 2014, 040901(R).
- [14] Glending P. Differential equations with bifocal homoclinic orbits. *Int. J. Bifurcation and Chaos*, **7**, 1997, 727-737.
- [15] Grebogi C., Ott E., Yorke J.A. Crises, sudden changes in chaotic attractors, and transient chaos. *Physica D*, **7**, 1983, 181-200.
- [16] Guckenheimer J., Holmes P. *Nonlinear oscillations, dynamical systems, and bifurcations of vector fields*. Springer, NY, 1983.
- [17] He K. Crisis-induced transition to spatiotemporally chaotic motions. *Phys. Rev. Lett.*, **80**, 1998, 696-699.
- [18] He K. Saddle pattern resonance and onset of crisis to spatiotemporal chaos. *Phys. Rev. Lett.*, **84**, 2000, 3290-3293.
- [19] He K. Critical behavior of crisis-induced transition to spatiotemporal chaos in parameter space. *Phys. Rev. E*, **63**, 2000, 016218.
- [20] He K. Riddling of the orbit in a high dimensional torus and intermittent energy bursts in a nonlinear wave system. *Phys. Rev. Lett.*, **94**, 2005, 034101.
- [21] He K., Chian A.C.-L. On-off collective imperfect phase synchronization and bursts in wave energy in a turbulent state, *Phys. Rev. Lett.*, **91**, 2003, 034102.
- [22] He K., Chian A.C.-L. Critical dynamics events at the crisis transition to spatiotemporal chaos. *Phys. Rev. E*, **69**, 2004, 026207.
- [23] He K., Chian A.C.-L. Nonlinear dynamics of turbulent waves in fluids and plasmas. *Nonlin. Processes Geophys.*, **12**, 2005, 13-24.
- [24] He K., Salat A. Hysteresis and onset of chaos in periodically driven nonlinear drift waves. *Plasma Phys. Controlled Fusion*, **31**, 1989, 123-141.
- [25] Kuznetsov Y.A. *Elements of applied bifurcation theory*. Springer, NY, 1998.

- [26] Laing C.R., Glending P. Bifocal homoclinic bifurcations. *Physica D*, **102**, 1997, 1-14.
- [27] Lopes S.R., Rizzato F.B. Nonintegrable dynamics of the triplet-triplet spatiotemporal interaction, *Phys. Rev. E*, **60**, 1999, 5375-5384.
- [28] Newhouse S., Ruelle D. and Takens F. Occurrence of strange Axiom A attractors near quasiperiodic flows on T^m , $m \geq 3$. *Comm. Math. Phys.*, **64**, 1978, 35-40.
- [29] Ott E. *Chaos in dynamical systems*. Cambridge Univ. Press, 2002.
- [30] Ovsyannikov I.M., Shilnikov L.P. Systems with a homoclinic curve of multidimensional saddle-focus and spiral chaos. *Mathematics of the USSR-Sbornik*, **73**, 1992, 415-443.
- [31] Peregrine D.H. Calculations of the development of an undular bore. *J. Fluid Mech.*, **25**, 1966, 321-330.
- [32] Podvigina O.M., Ashwin P.B. The $1 : \sqrt{2}$ mode interaction and heteroclinic networks in Boussinesq convection. *Physica D*, **234**, 2007, 23-48.
- [33] Press W.H., Teukolsky S.A., Vetterling W.T., Flannery B.P. Numerical recipes in Fortran. The art of scientific computing. Cambridge Univ. Press, 1992. 2nd ed.
- [34] Rempel E.L., Chian A.C.-L. Origin of transient and intermittent dynamics in spatiotemporal chaotic systems. *Phys. Rev. Lett.*, **98**, 2007, 014101.
- [35] Rempel E.L, Miranda R.A., Chian A.C.-L. Spatiotemporal intermittency and chaotic saddles in the regularized long-wave equation, *Phys. Fluids*, **21**, 2009, 074105.
- [36] Robert C., Alligood K.T., Ott E., Yorke J.A. Explosions of chaotic sets. *Physica D*, **144**, 2000, 44-61.
- [37] Ruelle D., Takens F. On the nature of turbulence. *Comm. Math. Phys.*, **20**, 1971, 167-192.
- [38] Toledo B.A., Chian A.C.-L., Rempel, E.L., Miranda, R.A., Muñoz P.R., Valdivia J.A. Wavelet-based multifractal analysis of nonlinear time-series:

the earthquake-driven tsunami of 27 February 2010 in Chile. *Phys. Rev. E*, **87**, 2013, 022821.

- [39] Yi F., Wei J., Shi J. Bifurcation and spatiotemporal patterns in a homogeneous diffusive predator-prey system. *J. Differential Equations*, **246**, 2009, 1944-1977.
- [40] Zheligovsky V.A. Numerical solution of the kinematic dynamo problem for Beltrami flows in a sphere. *J. Scientific Computing*, **8**, 1993, 41-68.

Table 3. Intervals of ϵ , for which exist some attractors from the family \mathcal{A}_l

Ω	\mathcal{A}_l	S_l	$P_l(F_1)$	$P_l(F_1/2)$	$P_l(F_1/4)$
0.56	(0, 0.103]	(0, 0.103]	--	--	--
0.57	(0, 0.115]	(0, 0.115]	--	--	--
0.58	(0, 0.128]	(0, 0.084], [0.104, 0.128]	[0.085, 0.103]	--	--
0.59	(0, 0.142]	(0, 0.07], [0.128, 0.142]	[0.071, 0.127]	--	--
0.60	(0, 0.156]	(0, 0.065], [0.146, 0.156]	[0.066, 0.145]	--	--
0.61	(0, 0.170]	(0, 0.065], [0.163, 0.170]	[0.066, 0.162]	--	--
0.62	(0, 0.186]	(0, 0.066], [0.18, 0.186]	[0.067, 0.179]	--	--
0.63	(0, 0.201]	(0, 0.069], [0.197, 0.201]	[0.07, 0.1608], [0.1644, 0.1689], [0.189, 0.196]	[0.1609, 0.1678], [0.169, 0.1769], [0.1843, 0.1889]	[0.177, 0.1842]
0.64	(0, 0.218]	(0, 0.074], [0.214, 0.218]	[0.075, 0.1649], [0.1778, 0.1786], [0.2082, 0.213]	[0.165, 0.1747], [0.1784, 0.1827], [0, 2062, 0.2081]	[0.1828, 0.1838], [0.2057, 0.2061]
0.65	(0, 0.2], [0.222, 0.234]	(0, 0.078], [0.231, 0.234]	[0.079, 0.1921], [0.2267, 0.234]	[0.1772, 0.1805], [0.1844, 0.1913], [0.2253, 0.2266]	[0.1914, 0.1921], [0.225, 0.2252]

Table 4. Intervals of ϵ , for which exist some attractors from the family \mathcal{A}_h

Ω	\mathcal{A}_h	S_h	$P_h(f_1)$	$T_h(f_1, f_2)$	$T_h(f_1, f_2/2)$	C_h
0.56	[0.063, 0.25]	[0.063, 0.0944]	[0.0945, 0.0951]	[0.0952, 0.0957]	[0.0958, 0.0959]	[0.09636, 0.25]
0.57	[0.067, 0.1], [0.110, 0.25]	[0.067, 0.0978]	[0.0979, 0.0985]	[0.0986, 0.0997]	[0.09976, 0.0998]	[0.110, 0.25]
0.58	[0.07, 0.1041], [0.129, 0.25]	[0.07, 0.101]	[0.102, 0.1022]	[0.1023, 0.103]	[0.1031, 0.1034]	[0.129, 0.25]
0.59	[0.073, 0.1085], [0.143, 0.25]	[0.073, 0.104]	[0.105, 0.106]	[0.107, 0.1077]	--	[0.143, 0.25]
0.60	[0.076, 0.112], [0.157, 0.25]	[0.076, 0.108]	[0.109, 0.1109]	[0.111, 0.1113]	--	[0.157, 0.25]
0.61	[0.079, 0.1165], [0.171, 0.25]	[0.079, 0.111]	[0.112, 0.114]	[0.115, 0.1155]	[0.1156, 0.1158]	[0.171, 0.25]
0.62	[0.082, 0.12047], [0.184, 0.25]	[0.082, 0.115]	[0.116, 0.118]	[0.119, 0.1197]	[0.1198, 0.112]	[0.184, 0.25]
0.63	[0.085, 0.1242], [0.197, 0.25]	[0.085, 0.118]	[0.119, 0.122]	[0.123, 0.124]	[0.1241, 0.1242]	[0.197, 0.25]
0.64	[0.088, 0.1282], [0.203, 0.25]	[0.088, 0.121]	[0.122, 0.125]	[0.126, 0.1279]	[0.128, 0.1282]	[0.203, 0.25]
0.65	[0.091, 0.1323], [0.202, 0.25]	[0.091, 0.1246]	[0.1247, 0.1295]	[0.1296, 0.132]	[0.1321, 0.1323]	[.202, .25]